

3-D mammary calcification reconstruction from a limited number of views

Andrew D.A. Maidment, Micheal Albert, Emily F. Conant, and Stephen A. Feig

Thomas Jefferson University, Department of Radiology
111 South 11th Street, Philadelphia, PA 19107

ABSTRACT

A method has been developed to allow mammographic differential diagnosis based upon the 3-D orientation and morphology of mammary calcifications. Two to seven digital radiographs of a cluster of calcifications are acquired on a prone stereotactic breast biopsy system. The images are segmented using a recursive region-growing algorithm. Inclusion of calcific material is dependent upon local statistics calculated over a region surrounding each calcification. Segmentation is aided by correlation of the calcifications in two or more views through analysis of their positions, sizes and shapes. The location of each calcification is determined geometrically; the shape of each calcification is calculated using the segmented images and a simulated annealing reconstruction method. Image segmentation and reconstruction can be reproducibly performed with an accuracy of 0.1 mm, which is sufficient to perform 3-D morphologic analysis. Biopsy specimens and *in vivo* calcifications have been examined. In instances where calcifications are associated with a mass, we can distinguish preferentially peripherally distributed calcifications from homogeneously distributed calcifications. We have also been able to elucidate the linear distribution of calcifications contained within the ductal system. In a preliminary ROC study involving 3 radiologists and 26 lesions (5 malignant), specificity increased when 3-D images were included in the diagnostic evaluation, resulting in an increase of A_z from 0.66 to 0.88 ($p = 0.0039$).

Keywords: digital mammography, stereomammography, mammary calcifications, image acquisition, image reconstruction, image segmentation, simulated annealing, ROC analysis

1. INTRODUCTION

Breast cancer is the most common cancer among women in the United States. In 1995, it was estimated that 182,000 new cases would be diagnosed and 46,000 women would die of the disease.^{1,2} There is evidence that both the mortality and morbidity resulting from breast cancer can be reduced with early detection.³⁻⁶ While many imaging modalities have been investigated for the diagnosis of breast cancer, film-screen mammography is currently the most sensitive modality available for the early detection of this disease.⁷⁻¹⁰ However, specificity is poor due to technical limitations, and the indeterminate radiographic appearance of many lesions. As a result, a large number of benign biopsies are performed. Only 1 in 4 biopsies will result in the detection of a cancer.¹¹ Benign biopsies represent a major expense and one of the largest deterrents to women entering a screening mammography program. A definitive, non-invasive method of distinguishing between benign and malignant breast lesions is essential.

The detection and differential diagnosis of subtle lesions using film-screen mammography is currently limited by insufficient film latitude, film granularity noise, and dose-inefficient scatter rejection.¹² First, the range of exposures present at the exit surface of the breast exceeds the range over which the gradient of film-screen combinations is near maximum (i.e., latitude), hence highly attenuating and highly transmissive regions of the breast are often imaged with sub-optimal contrast.^{12,13} Second, film granularity noise is nearly equal to x-ray quantum noise at zero spatial-frequency,¹⁴ reducing detection of low contrast objects (e.g., masses). At higher spatial-frequencies, the magnitude of film granularity noise exceeds that of x-ray quantum noise,^{14,15} reducing the detectability of small objects (e.g., calcifications). Finally, the use of a radiographic grid to reduce scattered radiation necessitates a 90 to 150% increase in dose to the breast.¹⁶ These technical limitations arise in part because the film serves as the detector, the image display device, and the image storage device. We have shown that these limitations of film-screen mammography imaging systems can be overcome with a digital imaging system.¹⁷ This is possible because the processes of acquisition, display and storage are performed independently and can be optimized separately.

Full-field digital mammography and the associated benefits will not be generally available for several years. We propose that a new paradigm be considered with regard to the application of digital mammography. It is our belief, that the most rapid implementation of digital mammography in the clinic will occur in the form of adjuvant diagnostic tools to film-screen mammography. There are several hundred small field-of-view digital mammography imaging systems installed in the United States for use in digital-mammography-guided stereotactic biopsies. We believe that such digital mammographic units provide an enormous, readily available resource for performing diagnostic "work-ups". Such work-ups could range from the simple use of the digital image receptor for magnified or non-magnified views of suspicious lesions, to digital stereomammography and 3-D reconstructed mammography. In this paper, we present one such method for improving the diagnostic specificity of the mammographic evaluation of clustered calcifications.

2. CLINICAL SIGNIFICANCE OF MAMMARY CALCIFICATIONS

Salomon¹⁸ was the first to report the mammographic presence of calcifications in a breast cancer. However, Leborgne¹⁹ was the first to recognize that calcifications can represent the only mammographic manifestation of a carcinoma. It has since been reported that between 29% and 48% of nonpalpable carcinomas are visible on the basis of calcifications alone.^{11,20-24} Calcifications are especially important as a sign of early breast cancer. Moskowitz²⁵ found that 71% of nonpalpable minimal cancers (noninfiltrating cancers and cancers smaller than 5 mm) were detected on the basis of calcifications alone. Feig *et al.*¹¹ and Anderson²⁶ found that 89% and 95%, respectively, of *in situ* ductal carcinomas were seen on the basis of calcifications alone.

Although certain types and patterns of calcifications are pathognomonic of malignant or benign lesions, so that biopsy is definitely indicated or contraindicated, in other instances the appearance is indeterminate, suggesting the possibility of carcinoma to varying degrees. A review of the literature reveals 25% to 36% of biopsies for calcifications are malignant.^{22,27-31} Thus, calcifications are sensitive but not specific cancer markers.

Several efforts have been applied to improve specificity through morphological studies. Some experts^{28,32} consider variation in size as suggestive of malignancy. A thin linear shape or a crystalline angulated shape is generally considered to be suspicious for ductal carcinoma.³³⁻³⁵ An irregular shape, contour, or margin of the calcifications are also suggestive of malignancy.^{31,32,35} Malignant calcifications have been described as typically dense^{33,36} but variations in density among calcific particles and within individual particles also seems to suggest malignancy.^{32,33} Several studies have shown a correlation between the number of calcifications in a cluster and the likelihood of a malignancy.^{28,30,37,38} Finally, distribution and spatial relationship are generally acknowledged to be extremely helpful guides to the need for biopsy. A linear or branching arrangement or one that is irregular and does not conform to anatomic planes is particularly suspicious for malignancy.^{31,33,34,39} Moreover, malignant calcifications are usually clustered and unilateral whereas benign calcifications are usually bilateral and symmetrically distributed.³²⁻³⁴

While qualitative rules, such as those described above, are routinely used in the differential diagnosis of breast lesions, such rules have not lead to dramatic improvements in specificity. In a seminal work⁴⁰, Lanyi has shown that the determination of malignancy has failed, in part, due to the processes of projection and superimposition that occur when any 2-D image is produced of a 3-D object. The result is a loss of information regarding the structure and morphology of breast lesions. Lanyi⁴⁰ advocated a 3-D morphologic analysis of breast calcifications to overcome these limitations and demonstrated the utility of this approach using a preliminary and invasive method. Our work in digital mammography^{17,41-47} and 3-D limited-view image reconstruction techniques⁴⁸ suggested that these two techniques could be combined to produce a non-invasive method of generating 3-D images of mammary calcifications from a limited number of views which would also overcome the limitations of film-screen mammography.⁴⁹⁻⁵⁴ In this paper, we describe such a method.

3. METHODOLOGY

The 3-D reconstruction of the calcification images is performed in a number of steps, beginning with acquisition of a limited number of projection images of the breast. Next, the calcifications are segmented from the background of breast parenchyma. The shape, size and position of each calcification in each view are used to determine the correspondence of the calcifications between the views. The 3-D location of each calcification is determined geometrically, and the 3-D

shape of each calcification is derived using a simulated annealing approach. Finally, the images are rendered in 3-D, and a morphologic analysis and mammographic differential diagnosis is performed.

3.1. Image acquisition

3-D images of calcifications are reconstructed from digital mammograms acquired on a prone stereotactic breast biopsy system (Fischer MammoTest™, Denver, CO). The biopsy system is fitted with a small field-of-view digital mammography detector (Fischer MammoVision™) that produces images which have a format of 1024 x 1024 pixels. Each pixel has a size of 48 μm, and is digitized as a 12 bit value. Images are acquired at the Thomas Jefferson University Breast Imaging Center. The images are then transferred to the University's Radiological Imaging Research Laboratory via ethernet using FTP.

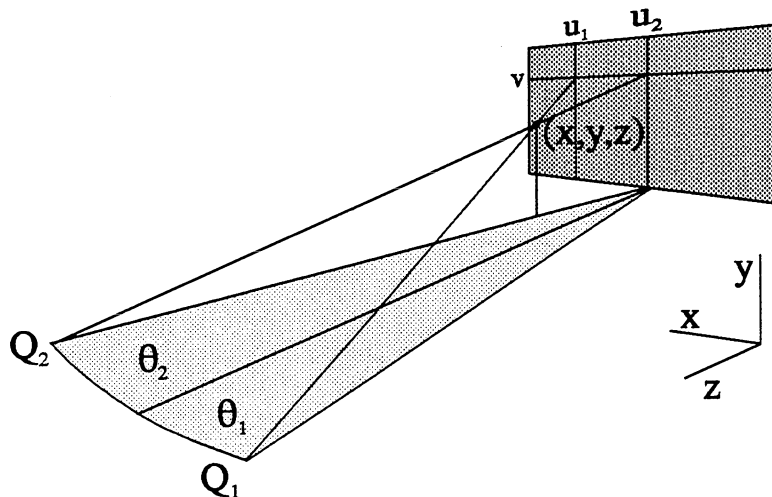
The image acquisition geometry is illustrated in Figure 1, where an object (x,y,z) is shown being imaged with the x-ray tube at point Q_1 , yielding a projection at (u_1,v) . Similarly, when the x-ray tube is at point Q_2 , the object is projected to (u_2,v) . A simple transformation from (u_1,u_2,v) to (x,y,z) is required to determine the 3-D location of the object. In routine usage of the biopsy system only 3 images are acquired (-15° , 0° and $+15^\circ$ relative to the perpendicular vector to the detector). In the clinical study discussed in Section 4.2, only two images were used (-15° and $+15^\circ$). However, as discussed in Section 4.1, a larger number of views may be acquired to improve the reconstructions. We have examined reconstructions which have used up to seven views of the breast, acquired in 15° increments from -45° to $+45^\circ$ (a total of 90° apart). A trade-off exists between the number of views and the dose incurred in the study. It is for this reason that CT of the breast is not performed. A study of the optimal number of views and acquisition angles is ongoing.

The mean glandular dose in the 3-D imaging procedure is similar to an average 2 view per breast mammography examination (2.5 mGy), and typically is less than is used in a magnification image of the breast. Each digital projection image of the breast is performed at a mean glandular dose of approximately 0.6 mGy. Thus the total mean glandular dose required to perform a 3-D study is between 1.8 mGy and 4.2 mGy, depending upon the number of views acquired.

3.2. Identification, segmentation, and correlation of multiple projection images

Currently, the calcifications in each image are identified manually. In this process, a seed point is placed near the center of a calcification by a human operator. The calcification is then segmented semi-automatically using a recursive region-growing algorithm. Next, the corresponding projected image of the calcification is identified in the second view, and the calcification is segmented. These steps are repeated for every calcification for which correspondence between the views is found.

Figure 1: An illustration of the image acquisition geometry. When the x-ray tube is at position Q_1 the image of the calcification is projected onto the detector (dark gray) at a point (u_1,v) , and at position Q_2 the image is projected to (u_2,v) .



The segmentation algorithm assumes that the seed point is located near the center of the calcification. Any pixel adjacent to the seed point with a digital value significantly below the local average is added to the segmented region, and pixels adjacent to these pixels are in turn tested. The local average is calculated as the mean signal intensity of the 50x50 pixel region centered on the seed point, and pixels are considered to be significantly below the average if they are less than the average by more than four times the local noise. This local noise is computed by dividing the 50x50 pixel region into 4x4 sub-regions, calculating the RMS value in each sub-region, then taking the median of the RMS values. Next, a "background region" surrounding each calcification is calculated. This region is used to estimate the intensity of the signal that would occur in the absence of calcific material at each pixel in the segmented calcification. This signal is denoted I_{bg} . The attenuation due to calcium can then be calculated as $I_{ca} = I_{bg} - I_{obs}$, where I_{obs} is the observed intensity of the signal in the calcific pixel prior to subtraction.

It is possible to correlate the projected image of each calcification in the different views of the breast from the positions, shapes and sizes of the projected images. Note, for example, that the two projected positions $[(u_1, v)$ and $(u_2, v)]$ of a calcification at position (x, y, z) share a common coordinate, v , as shown in Figure 1. It is possible, therefore, to use the mass of the calcifications that span a similar range of v values to determine which projected shadow corresponds to which calcification in each view. By adding additional views, one can then verify the calculated 3-D position against the segmented calcifications in those views, as well as identifying those calcifications which are hidden or obscured in one or more of the other views. In this manner, it is possible to identify each calcification in each view.

3.3. Reconstruction of 3-D image data

In this process, we separately determine the 3-D location and the 3-D shape of each calcification. The 3-D location is determined geometrically. The 3-D shape of each calcification is determined using the segmented image data in conjunction with a simulated annealing reconstruction method.

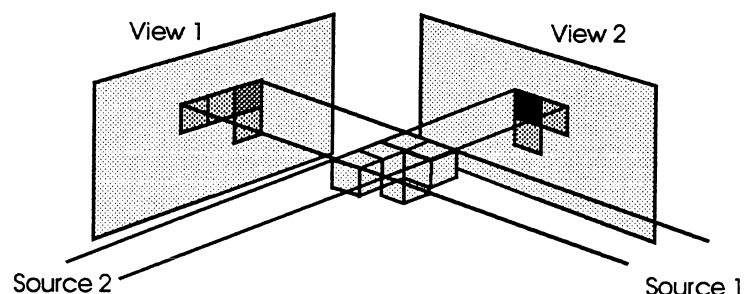
3.3.1. Determination of 3-D location

As illustrated in Figure 1, an object at point $C = (x, y, z)$ will produce a projection at $P_1 = (u_1, v)$ when viewed with the first x-ray source at point Q_1 , and will produce a projection image at $P_2 = (u_2, v)$ when viewed with the x-ray source at point Q_2 . The line P_1Q_1 and P_2Q_2 lie in the plane Q_1Q_2C , and meet at the point C , which is the position of the calcification. These simple geometric considerations allow one to calculate the coordinates of C .

3.3.2. Determination of 3-D shape

The intensity of the signal in each pixel of each view of the breast is dependent upon the amount of calcific material (and other breast tissues) in the path of the x-rays that contribute to signal at that pixel. This concept is illustrated in Figure 2, where a simulated object of equally attenuating cubes is held *in vacuo*, and imaged with an idealized imaging

Figure 2: A simplified illustration of the reconstruction problem. A object (treated as a set of voxels containing calcium) is shown in two projections. Note, that the intensity of the projection is related to the number of voxels traversed which contain calcium, and that the object is contained within the intersection of the back-projections (the image mask).



system in a non-divergent geometry. The intensity of the signal in the image depends upon the number of cubes transversed. To determine the 3-D shape of the object from the projection data requires an inverse transformation technique. We have chosen a simulated annealing method to which certain *a priori* constraints have been added.

In order to reconstruct the shape of the calcification, the space about the calcification is divided into voxels. Reconstruction begins by identifying all voxels whose projections are geometrically consistent with all of the observed shadows. Only voxels in this mask are eligible for inclusion in the final reconstruction. When 3 or more views of the breast are available with sufficient angular distribution, we apply a simulated annealing technique to reconstruct the calcification. When the views are within ± 15 degrees of each other the difference in perspective is insufficient to define the shape of the object. In this case the masked voxels form a solid which is elongated in the direction perpendicular to the image plane (the *z* axis), which is *a priori* an unlikely shape. To correct this we apply the following heuristic: observing that in each plane parallel to the *xz* plane (the *x* direction is parallel to the displacement between x-ray tube positions between exposures) the mask appears as a trapezoid, any voxel in this plane whose distance from the center of the trapezoid is greater than the average distance of the four sides from the center of the trapezoid is excluded.

When multiple views are available, we can apply the simulated annealing algorithm show in Figure 3. Every possible shape of the calcification is associated an "energy" function of the form

$$\chi^2 = \sum (t_{calc} - \ln(I_{bg}/I_{obs}))^2 \quad (1)$$

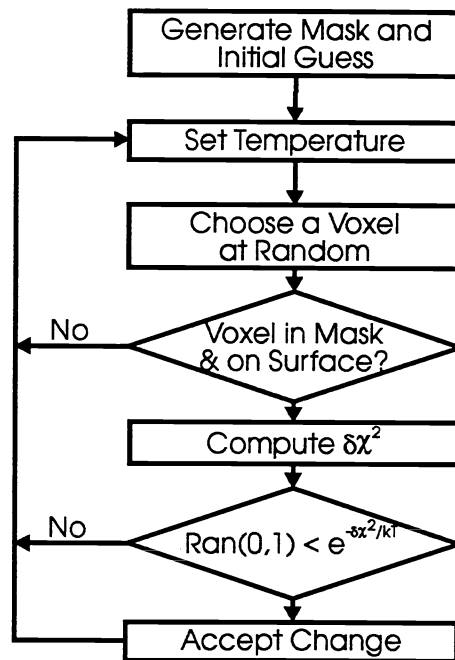
which measures how poorly the given shape reproduces the observed shadows. Here I_{obs} represents the digital value measured in a pixel, I_{bg} is the estimated value which would have been observed at that position in the absence of the calcification, t_{calc} is the length of intersection of the calcification with the line running from the x-ray source to the pixel, and the sum is taken over all points in the 50 x 50 pixel region. In order to estimate I_{bg} for pixels in the calcification, a linear fit is made to the digital values in a ring of pixels between 3 and 6 pixels away from the boundary of the calcification. Outside the calcification $\ln(I_{bg}/I_{obs}) = 0$ by definition. In these calculations the effective attenuation length of the material constituting the calcification is taken as a parameter to be fitted to account for the varying consistencies of the calcific materials, the effects of beam hardening through different thicknesses of tissue in the different views, and the effect of scatter.

The mask computed above is used as the starting configuration for a simulated annealing process. At each step of this process a voxel is randomly chosen such that, if it is in the calcification, it has at least one neighbor outside the calcification, and if it is outside the calcification, it has at least one neighbor inside. The effect on the energy function, $\delta\chi^2$, of changing the state of the chosen calcification is then computed. The probability of the change actually occurring is given by

$$e^{-\delta\chi^2/kT} \quad (2)$$

where kT is a unitless quantity which represents the effective temperature at each stage of the annealing process. Thus initially the search explores a wide range of configurations, most of which do not fit the data well. As the process continues, the effective temperature is reduces and the search is restricted to a smaller region of the relevant phase space. In this manner, a 3-D reconstruction of each calcification is made.

Figure 3: Flowchart of the simulated annealing process. Details of the process are described in the text.



3.4. Rendering of 3-D image data

Once the list of voxels constituting the reconstruction of the calcification is obtained, the surface is approximated for the purpose of 3-D rendering using the marching cubes algorithm.⁵⁵ Rendering is performed using the PEX extension to the X Window System. Objects are rendered in perspective with shading appropriate for both diffuse and specular reflection from both directional and diffuse light sources. The 3-D images may be viewed monoscopically or as stereoscopic anaglyphs. To produce anaglyphs, PEX is used to produce two images in different colors and different perspectives, which are then additively superimposed pixel-by-pixel.

4. RESULTS AND DISCUSSION

4.1. Image segmentation and reconstruction

We have demonstrated that image segmentation and reconstruction can be reproducibly performed with an accuracy of ± 0.1 mm, which is sufficient to produce accurate 3-D images of the calcification clusters for the radiologists, and to allow 3-D morphologic analysis of the calcifications.

An example of the results of the simulated annealing algorithm is shown in Figure 4. In computing this example, a 400 μm diameter sphere with a large cavity was simulated and additively superimposed upon experimentally acquired digital images of a uniform lucite test phantom. Images of the phantom were acquired at angle between -45° and 45° , in 15° increments. Images of the object were simulated at the same angles. X-ray quantum noise was evident in the images and was maintained in simulated images of the object. The cavity was oriented away from the x-ray tube 0° position, thus the 2-D images of the object appear disk-like. The simulated calcification is shown from several perspectives in the first column of Figure 4. The following columns show the results of reconstruction by simulated annealing using information from 3, 5, and 7 views, viewed from the same perspectives. In all cases the reconstruction shows an object which is basically round with a distinct depression on the same side as the simulated calcification, so that the morphology of the calcification is preserved in the reconstruction. As the number of views increases this shape becomes qualitatively clearer. For the 7 view reconstruction the overlap between the reconstructed volume and the volume of the simulated calcification is 90% of the volume of the calcification. The discrepancy consists almost entirely of voxels on the surface of the calcification. Given the pixel size of the detector, the error in the position of the boundary can not be smaller than $\sim 25 \mu\text{m}$. For a 200 μm radius sphere, a 25 μm skin accounts for 30% of the volume, so surface voxels affect the overlap volume significantly more than might be expected. These voxels do not, however, impede the ability to identify this object as having a cavity which would not be evident when viewing the 2-D images.

4.2. Clinical evaluation

3-D images of more than 30 cases of clustered calcification have been generated with the above method. Images of both breast biopsy specimens containing calcifications, and *in vivo* calcifications have been acquired. Anecdotally, we have observed that in instances when the calcifications are associated with a mass, it has been possible to distinguish preferentially peripherally distributed calcifications from homogeneously distributed calcifications. This is possible in spite of the fact that in the 3-D renderings there is no frame of reference in which the reader can relate the calcifications to the mass. This observation is very important, because preferentially peripherally distributed calcifications are predominately associated with benign diseases, while clustered malignant calcifications are often homogeneously or linearly distributed calcifications, although not all such calcifications are malignant.

It has also been possible to elucidate the ductal distribution of some malignant calcifications using the 3-D reconstruction technique. An example of a calcification cluster which demonstrates a ductal distribution is shown in Figure 5. In Figure 5-A, two digital mammographic views (-15° , and $+15^\circ$) of the calcification cluster can be seen. The image depicts an area 2.5 cm x 2.5 cm. In Figure 5-B, the calcifications which were segmented from each image are shown. Finally, in Figure 5-C, a stereoscopic image pair of the 3-D image of the calcification cluster is shown. The angle of the image pair in Figure 5-C does not correlate to either of the above views, but rather was chosen to clearly demonstrate the ductal distribution. In this case, we were able to segment 40 calcifications, which demonstrate the characteristic linear arrangement of a ductal carcinoma.

Figure 4: Reconstructions of a simulated 400 μm diameter calcification are shown (from left to right) for the original object and for reconstructions using 7 views, 5 views, and 3 views. The following views were used: 7 ($\pm 45^\circ$, $\pm 30^\circ$, $\pm 15^\circ$, $\pm 45^\circ$, $\pm 30^\circ$ and 0°), and 3 ($\pm 45^\circ$ and 0°). The object is viewed at three different angles (from top to bottom) to show the spherical side, the concavity in profile, and the concavity.

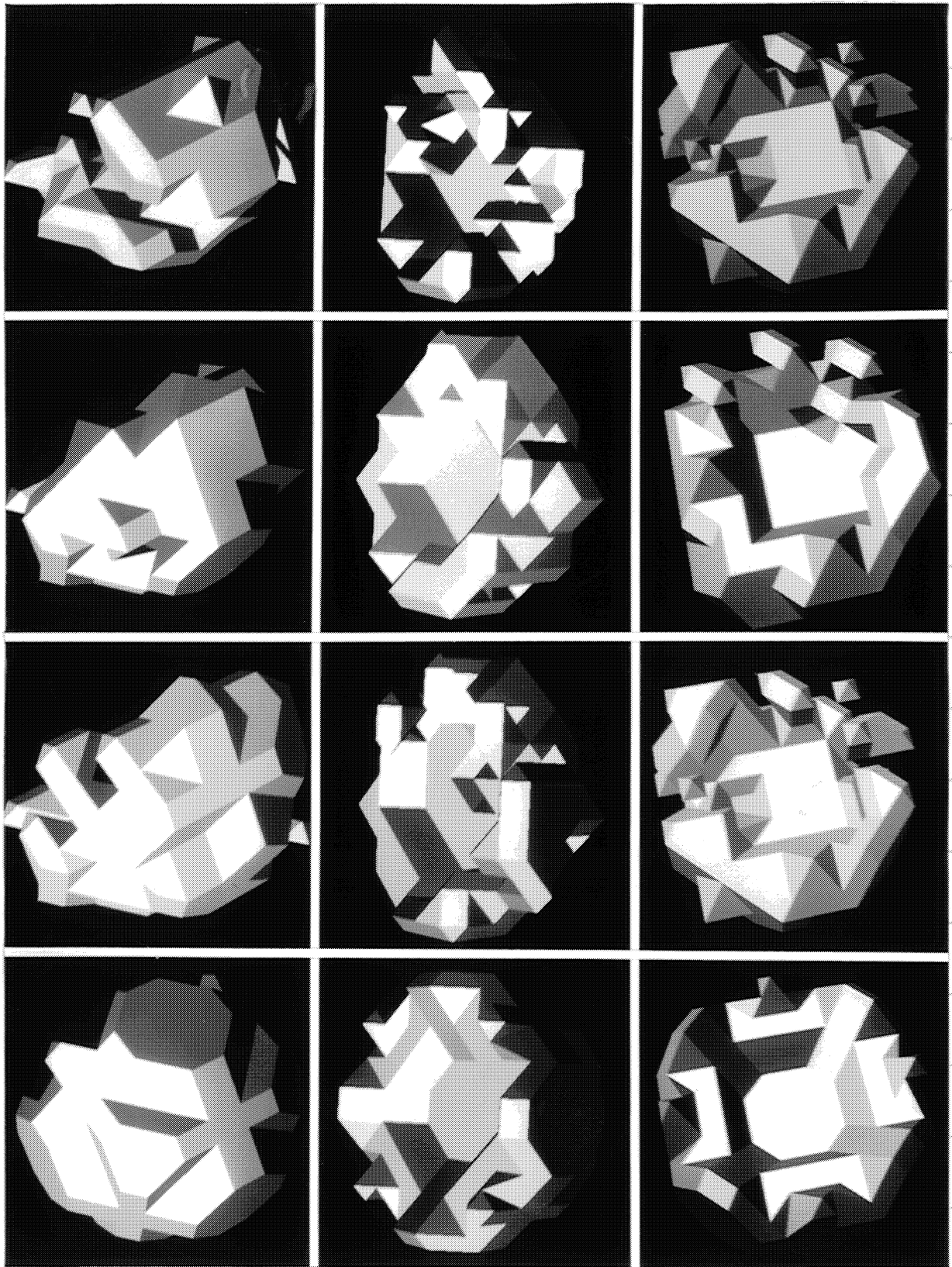


Figure 5: A example of an *in vivo* calcification cluster imaged using the stereotactic digital mammography imaging system. Images taken at two different angles are shown in A (-15° left and $+15^\circ$ right). The calcifications identified and segmented from the two views are shown in B. A 3-D stereoscopic image pair are shown in C. The view in C was chosen to optimally display the 3-D orientation and does not correspond to either view in A or B. The perception of 3-D can be achieved by placing C approximately 20 cm from your eyes, and focusing your eyes as if viewing a distant object.

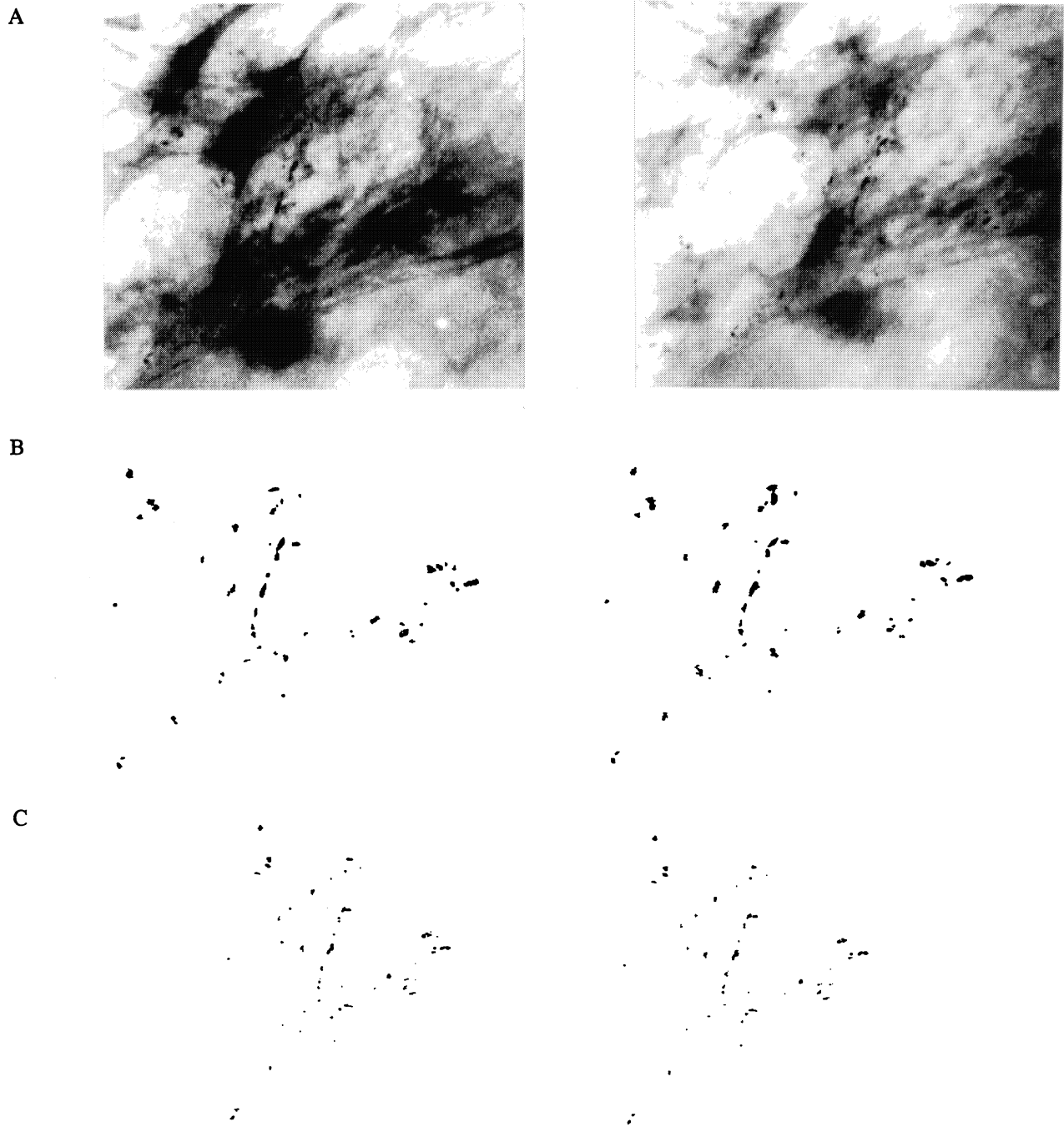
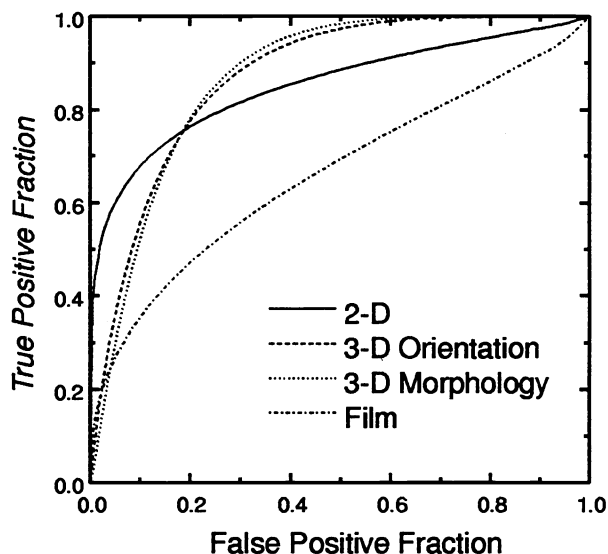


Figure 6: Results of the ROC analysis of 26 cases (5 malignant). The results are shown for four types of clinical review: film only, or with the addition of 2-D digital, 3-D cluster orientation, and 3-D cluster orientation and calcification morphology.



A preliminary study of 26 cases was performed to quantify the utility of the 3-D reconstruction technique. In this study, we compared the appearance of clustered calcifications in film-screen mammograms, digital mammograms and digital 3-D images. The "film images" included film-screen mammograms, magnified film-screen mammograms, and needle localization and biopsy specimen films, or digital stereotactic core biopsy film records and core biopsy specimen films. Eight of the cases were of *in vivo* calcifications for which core biopsies were performed. Eighteen of the cases were breast biopsy specimens, following excisional biopsy. In the excisional breast biopsy cases, the specimens were placed in a plastic container with sufficient water to simulate a 4.5 cm thick breast. In all cases, the average signal intensity was approximately 3000 digital units, indicating a similar detector exposure was used in each case. Of the 26 cases, 22 had complete film-screen mammographic studies available for review; 4 only had films related to the needle placement (2 orthogonal needle placement films and contact radiographs of the biopsy specimen). In one instance, the clustered calcifications were partially obstructed in one of the two views.

In the study, three radiologists separately reviewed each case. Five of the cases were malignant, the remainder were benign. In each case, the radiologist was presented with the film images of the study. The radiologists were asked to rate each case on a modified "degree of suspicion" scoring system; 5 = definitely malignant, 4 = probably malignant, 3 = suspicious for malignancy, 2 = probably benign, and 1 = definitely benign. A score of 3 or higher would indicate a biopsy procedure was necessary. The radiologists were also presented with the 2-D digital images which were acquired for each case. Again, the readers rated each case, after having altered the display window and level and electronic magnification (pixel replication) as desired. The radiologists were then presented with the 3-D images and asked to rate each case, by considering the 3-D orientation of the cluster only. Finally, the radiologists were asked to rate each case examining the 3-D orientation of the cluster and the morphology of the individual calcifications.

The results of the three radiologists were pooled and analyzed using ROC methodology, and are presented in Figure 6. We found that the specificity of diagnosis (benign vs. malignant) as indicated by the area under the ROC curve, increased from $A_z = 0.66$ for film-screen mammograms to $A_z = 0.88$ when all techniques were included in the diagnostic evaluation ($p = 0.0039$). The complete ROC results are shown in Table 1. While there is little difference between the A_z values for the different digital methods, there was a significant difference in the number of benign biopsies which could have been avoided if the 3-D imaging technique had been used to determine the necessity of the biopsies. A biopsy was considered "avoidable" if the score was 1 or 2. These data are also included in Table 1. In no case was a malignant calcification cluster downgraded below a score of 3, so that there was never a case where a biopsy would not have been performed on a malignant cluster.

Method	A_z	% of benign biopsies which were avoidable
Film-Screen	0.6565 ± 0.0990	11.1%
2-D Digital	0.8507 ± 0.0703	33.3%
3-D Orientation	0.8689 ± 0.0530	40.9%
3-D Orientation and Morphology	0.8750 ± 0.0477	50.0%

Table 1: A summary of the results of a preliminary clinical evaluation of 2-D and 3-D digital imaging of calcifications. The digital methods resulted in a increase in the area under the ROC curve (A_z), and a decrease in the number of biopsies which were felt to be necessary by the radiologists.

6. CONCLUSION

In conclusion, we propose a new paradigm be espoused in which existing digital mammography imaging systems are used as an adjuvant tool to film-screen mammography. We have developed one such method which produces 3-D images of clustered mammary calcifications. This technique uses images which are acquired on a small field-of-view digital mammography prone stereotactic biopsy system. The 3-D images are produced using a method that includes identification, segmentation and correlation of each calcification in the breast in a limited number of projection images of the breast, and subsequent reconstruction of the calcifications from these views. The dose in this procedure is comparable to that used in magnification mammography. In a preliminary clinical evaluation we have demonstrated that 3-D morphologic analysis of calcifications is possible and can significantly increase specificity and decrease the number of biopsies required.

7. ACKNOWLEDGEMENTS

This research was supported by a grant from the Research and Education Fund of the Radiological Society of North America. Additional support has been provided from the Radiology Research Fund of Thomas Jefferson University. This work is conducted under the auspices of the National Digital Mammography Development Group. The authors wish to thank Dr. Catherine Piccoli, Dr. Steven Nussbaum, Dr. Elaine Wolk, and Ms. Lisa Fisher of Thomas Jefferson University for their assistance with this project, Dr. Martin Yaffe and Mr. Normand Robert of the University of Toronto, and Dr. Robert Nishikawa of the University of Chicago for their insightful comments.

9. REFERENCES

1. American Cancer Society. Cancer facts and figures 1995. Atlanta, GA, American Cancer Society, 1995.
2. Wingo PA, Tong T and Bolden S. Cancer statistics 1995. *CA* 45:8-30, 1995.
3. Seidman H *et al.* Survival experience in the Breast Cancer Detection Demonstration Project. *Ca*. 37:258-290, 1987.
4. Feig SA. Decreased breast cancer mortality through mammographic screening: Results of clinical trials. *Radiology* 167:659-665, 1988.
5. Shapiro *et al.* Current results of the breast cancer screening randomization trial: The Health Insurance Plan (HIP) of Greater New York, in NE Day and AB Miller (Eds) *Screening for Breast Cancer*, Toronto, Hogrefe, 1988.
6. Tabar L *et al.* Update of the Swedish two-county program for mammographic screening for breast cancer. *Radiol. Clin. N. Am.* 30:187-210, 1992.
7. Kopans DB *et al.* Breast Imaging. *NEJM* 130:960-967, 1984.
8. Sickles EA. Breast Imaging: A view from the present to the future. *Diagn. Imag. Clin. Med.* 54:118-125, 1985.
9. Kopans DB. Non-mammographic breast imaging techniques. *Rad Clin N Am* 25:961-971, 1987.
10. Kopans DB. Priorities for improved breast cancer imaging, in AG Haus and MJ Yaffe (eds) *Technical aspects of Breast Imaging*, RSNA, Oakbrook IL, 271-274, 1994.

11. Feig SA, Shaber GS, Patchefsky A, *et al.* Analysis of clinically occult and mammographically occult breast tumors. *AJR* 128:403-408, 1977.
12. Nishikawa RM *et al.* Scanned projection digital mammography. *Med Phys* 14:717-727, 1987.
13. Sabol JM and Plewes DB. Latitude limitations of film-screen mammography. *Med Phys* 18:1076, 1991.
14. Bunch PC *et al.* Sources of noise in high-resolution screen-film radiography. *Proc SPIE* 626:64-75, 1986.
15. Nishikawa RM and Yaffe MJ. SNR properties of mammographic film-screen systems. *Med Phys* 12:32-39, 1985.
16. Dance DR *et al.* Calculation of dose and contrast for two mammographic grids. *Phys Med Biol* 37:235-248, 1992.
17. Maidment ADA. *Scanned-slot digital mammography*. Ph.D. Thesis, University of Toronto, Toronto, Canada, 1993.
18. Salomon A. Beitrage zur pathologie und klinik der marmakarzinome. *Arch Klin Chir* 101:573-668, 1913.
19. Leborgne R, Dominguez CM, Mautone JA. Diagnostico de los tumores de la mama por la radiografia simple. *Boletin de la Sociedad de Cirugia del Uruguay* 20:407-422, 1949.
20. Wolfe JN. Analysis of 462 breast carcinomas. *AJR* 121: 846-853, 1974.
21. Frischbier H-J, Lohbeck HU. *Fruhdiagnostik des Mammakarzinoms*. Thieme, Stuttgart, 1977.
22. Bjurstam N. Radiology of the female breast and axilla. *Acta Radiol Suppl* 357, 1978.
23. Menges V, Busing CM, Hirsch O. *RoFo* 135:372-378, 1981.
24. Frankl G, Ackerman M. Xeromammography and 1200 breast cancers. *Radiol Clin North Am* 21:81-91, 1983.
25. Moskowitz M. The predictive value of certain mammographic signs in screening for breast cancer. *Cancer* 51:1007-1011, 1983.
26. Anderson I. Mammographic screening for breast carcinoma. Ph.D. Thesis, Malmö, 1980.
27. Murphy WA, DeSchryver-Kecsckemeti K. Isolated clustered microcalcifications in the breast. *Radiology* 127: 335-341, 1978.
28. Egan RL, McSweeney MB, Sewell CW. Intramammary calcifications without an associated mass in benign and malignant diseases. *Radiology* 137:1-7, 1980.
29. Sickles EA. Further experience with microfocal spot magnification mammography in assessment of clustered breast microcalcifications. *Radiology* 137:9-14, 1980.
30. Muir BB, Lamb J, Anderson TJ, *et al.* Microcalcification and its relationship to cancer of the breast. *Clin Radiol* 34:193-200, 1983.
31. Sigfusson BF, Andersson I, Aspegren K, *et al.* Clustered breast calcifications. *Acta Radiologica* 24: 273-281, 1983.
32. Tabar L, Dean PB. *Teaching atlas of mammography*. Thieme, Stuttgart, 1983.
33. Hoeffken W, Lanyi M. *Mammography*. Saunders, Philadelphia, 1977.
34. Martin J. *Atlas of Mammography*. Williams and Wilkins, Baltimore, 1982.
35. Wolfe JN. *Xeroradiography of the breast*. Thomas, Springfield IL, 1983.
36. Millis RR, Davis R, Stacey AJ. Detection and significance of calcifications in the breast. *Br J Radiol* 49:12-26, 1976.
37. Rogers JV, Powell RW. Mammographic indications for biopsy of clinically normal breasts. *AJR* 115: 794-800, 1972.
38. Menges V, Wellauer J, Engeler V, *et al.* *Radologe* 13:468-476, 1973.
39. Moskowitz M. Screening is not diagnosis. *Radiology* 133:265-268, 1979.
40. Lanyi M. *Diagnosis and Differential Diagnosis of Breast Calcifications*. Springer-Verlag, New York, 1988.
41. Farhig R, Maidment ADA and Yaffe MJ. Optimization of peak kilovoltage and spectral shape for digital mammography. *Proc SPIE* 1651:74-83, 1992.
42. Maidment ADA and Yaffe MJ. Scanned-slot digital mammography. *Proc SPIE* 1231:316-326, 1990.
43. Maidment ADA and Yaffe MJ. Analysis of the spatial-frequency-dependent DQE of optically-coupled digital mammography detectors. *Med. Phys.* 21:721-729, 1994.
44. Maidment ADA, Yaffe MJ, Plewes DB, *et al.* Imaging performance of a prototype scanned-slot digital mammography system. *Proc. SPIE* 1896:93-103, 1993.
45. Maidment ADA, Fahrig R and Yaffe MJ. Dynamic range requirements in digital mammography. *Med. Phys.* 20:1621-1633, 1993.

46. Maidment ADA and Yaffe MJ. Analysis of signal propagation in optically-coupled detectors for digital mammography: 1. Phosphor screens. *Phys. Med. Biol.* **40**:877-889, 1995.
47. Maidment ADA and Yaffe MJ. Analysis of signal propagation in optically-coupled detectors for digital mammography: 2. Optical-coupling efficiency. *Phys. Med. Biol.* **41**(3), 1996.
48. Robert N, Peyrin F and Yaffe MJ. Binary vascular reconstruction from a limited number of projection images. *Med Phys.* **21**:1839-1851, 1994.
49. Robert N, Maidment ADA, and Yaffe MJ. Three-dimensional localization and display of breast microcalcifications. *Proc annual meeting division of medical and biological physics of the Canadian association of physics.* London Ontario, 1989.
50. Maidment ADA and Seshagiri S. Method for 3-D morphologic analysis of breast calcifications. *Radiology* **193P**:200, 1994.
51. Maidment ADA, Conant EF, Seshagiri S and Feig SA. Three-dimensional morphologic analysis of breast calcifications. *Radiology* **193P**:217, 1994.
52. Maidment ADA, SA Feig and Conant EF. The three-dimensional morphological analysis of breast calcifications. *Med. Phys.* **21**:988, 1995.
53. Maidment ADA, Feig SA, Conant EF, Wolk E, and Albert M. 3-D analysis of breast calcifications. *Radiology* **197P**:170, 1995.
54. Maidment ADA, Conant EF, Feig SA, and Albert M. Segmentation and 3-D reconstruction of breast calcifications for morphologic analysis. *Radiology* **197P**:327-8, 1995.
55. Lorensen WE and Cline HE. Marching cubes: A high resolution 3D surface construction algorithm. *ACM Computer Graphics* **21**:163-169 1987.